

REVIEW

[View Article Online](#)
[View Journal](#)


Cite this: DOI: 10.1039/c9qm00043g

Structural colors in metasurfaces: principle, design and applications

Bo Yang,^a Hua Cheng,^{ab} Shuqi Chen^{id}*^{abc} and Jianguo Tian^{ab}

Structural colors resulting from the interference between incident light and structures are ubiquitous in nature and daily life. In contrast to conventional chemical pigments and dyes, structural colors have the advantages of low consumption, environmental protection and high durability. To reach higher resolutions beyond diffraction limits, structural colors based on metasurfaces consisting of artificially designed nanoresonators at subwavelength scale have been proposed in recent years. In this review, we classify structural colors into plasmonic colors and dielectric colors according to different mechanisms, summarizing the development and applications for a variety of color filters. Moreover, four significant methods of dynamically tunable colors are discussed, including mechanical stretching, chemical reaction, electrical control, and photon doping.

Received 25th January 2019,
Accepted 24th February 2019

DOI: 10.1039/c9qm00043g

rsc.li/frontiers-materials

1. Introduction

Colors as important visual carriers in our daily lives have been widely studied since prehistoric times. 140 years ago, the discovery of mauveine by W. H. Perkin promoted development of the extensive synthetic dyes and pigments industry.¹ So far,

synthetic colorants have been used in decorations, synthetic fibers, printing inks and identification, for example.^{2–4} In particular, organic pigments are finding increasing use in high-technology industries, such as optoelectronic displays, optical data storage and photo-reprographics (Fig. 1a).⁴ However, from the perspective of recycling, chemical colorants are costly and environmentally damaging. In addition, their insufficient resolution and lack of durability invariably limit their practical applications in displays and images.^{5,6}

To overcome these limitations, considerable attention has been paid to structural colors, which are an interference phenomenon between incident light and structures. Structural colors are ubiquitous in nature and daily life, such as in beetles, Pollia fruits, peacocks, hummingbirds, morpho butterflies

^a The Key Laboratory of Weak Light Nonlinear Photonics, Ministry of Education, School of Physics and Teda Institute of Applied Physics, Nankai University, Tianjin 300071, China. E-mail: schen@nankai.edu.cn

^b Renewable Energy Conversion and Storage Center, Nankai University, Tianjin 300071, China

^c The Collaborative Innovation Center of Extreme Optics, Shanxi University, Taiyuan, Shanxi 030006, China



Bo Yang

Bo Yang is currently a PhD student of Prof. Shuqi Chen at the Key Laboratory of Weak Light Nonlinear Photonics, Ministry of Education, School of Physics and Teda Institute of Applied Physics, Nankai University, China. She received her bachelor's degree in materials physics from Nankai University in 2016. Her current research focuses on dielectric metasurfaces and structural colors.



Shuqi Chen

Shuqi Chen is a professor at the Key Laboratory of Weak Light Nonlinear Photonics, Ministry of Education, School of Physics and Teda Institute of Applied Physics, Nankai University, China. He received his joint training PhD degree from the University of Arizona, USA, and Nankai University, China, in 2009. He is a winner of New Century Excellent Talents Support Program of the Ministry of Education of China in 2013. Prof. Chen's current research interests include nonlinear optics, phononics and acoustics metasurfaces, and subwavelength electromagnetics.

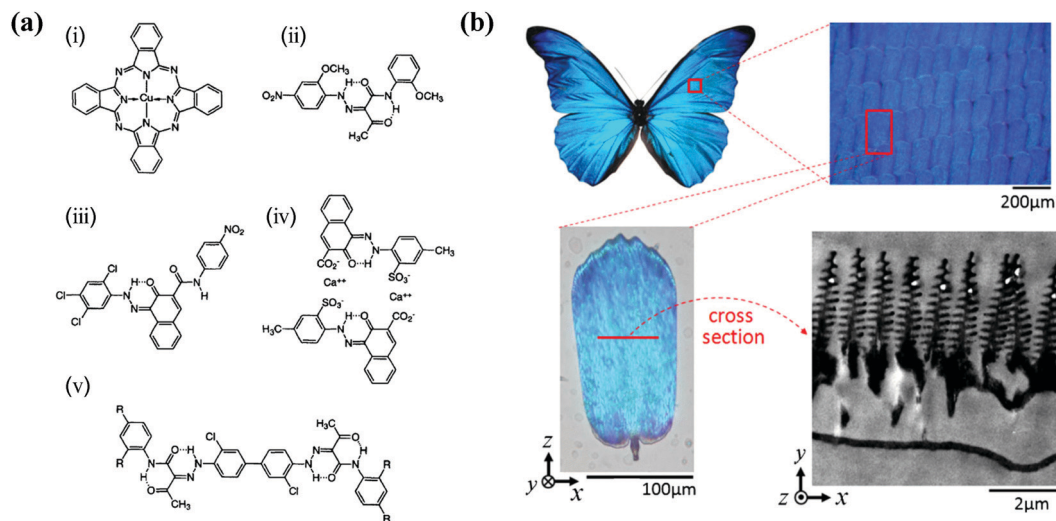


Fig. 1 (a)(i)–(v)) Chemical structures of some typical classical pigments. a(i) C. I. Pigment Blue 15, a(ii) C. I. Pigment Yellow 74, a(iii) C. I. Pigment Red 112, a(iv) C. I. Pigment Red 57:1, a(v) C. I. Pigment Yellow 12 (R=CH₃) and C. I. Pigment Yellow 12 (R=H). Reproduced from ref. 4, with permission from Royal Society of Chemistry journal, Copyright 1997. (b) Structural colors of male *Morpho rhetenor* wings. The enlarged image presents the ridges and lamellae alignments on the cross-section of the wings. Reproduced from ref. 11, with permission from Optical Society of India, Copyright 2012.

and so on.^{7–10} For instance, reflected light from the complex nanoridges and lamellae in the morpho rhetenor wings exhibits bright metallic blue, as shown in Fig. 1b.¹¹ Compared with chemical pigments, structural colors have the advantages of (1) showing brighter colors under sunlight, (2) higher resolutions, (3) the ability of dynamic tuning by changing surface structures, and (4) better durability under high-temperature and high-intensity illumination.^{12–14} In general, structural colors are generated from different bulk materials including light scattering, photonic crystals and multilayer materials.^{12,15,16} Nevertheless, owing to bulk effects, high-quality colors always require more particles, larger periods and added layers, indicating that the thickness of color structures is much greater than the wavelength.^{11,15} As a result, there is still considerable room to further improve the resolution of structural colors beyond the diffraction limit.

In this context, a metasurface as a two-dimensional (2D) artificial structure at a subwavelength scale is a good candidate for the generation of high-resolution structural colors. Controlled optical properties can be introduced by engineering the geometric parameters of the periodic resonators array. According to the type of material of the resonators, metasurfaces can be classified into plasmonic and dielectric metasurfaces. For plasmonic metasurfaces, optical responses are mainly driven by plasmonic resonance based on a variety of metallic nanostructures.^{17–20} In contrast, for dielectric metasurfaces, electric and magnetic-dipole resonances generated from high-index dielectric materials simultaneously simulate novel optical phenomena.^{21–23} So far, with the development of micro-nano fabricated techniques, a number of unprecedented optical properties based on metasurfaces have been demonstrated to control and guide electromagnetic waves from microwaves to the visible range, such as the spin Hall effect,^{24,25} anomalous refraction,^{26,27} nonlinear optics^{28–30} and, in particular, structural colors.

In this review article, we focus on the development of structural colors generated from plasmonic and dielectric metasurfaces on the basis of principle, design and applications. A variety of color filters with different nanostructures and materials are systematically analyzed and summarized from the static state to the dynamic state. The methods of dynamically tunable colors are discussed, including mechanical stretching, chemical reaction, electrical control and photon doping. In addition, we also introduce practical applications of color filters, such as high-end displays, encryption and colorimetric sensing, indicating the wide prospects in real life.

2. Color generation from metasurfaces

2.1 Colors from plasmonic metasurfaces

Surface plasmons (SPs), the collective oscillation of free electrons and photons at the interfaces of metal and dielectric materials, have shown the unprecedented properties of strongly enhanced local field and in-plane momentum.^{31–33} SP generated from plasmonic metasurfaces plays a vital role in many applications, such as optical holograms,^{34,35} waveguides,³⁶ flat lenses,³⁷ directional couplers,³⁸ waveplates^{39,40} and so on. In particular, one of the most intriguing areas of research in recent years is the study of plasmonic structural colors. The plasmonic resonance by coupling between SP and incident light can selectively filter visible light in transmission or reflection mode. To date, many plasmonic additive and subtractive color filters beyond the sub-wavelength diffraction limit have been extensively reported due to high resolution, ease of fabrication and high flexibility at the subwavelength scale.^{40–49} In this section, some typical plasmonic nanostructures composed of nanogratings, nanoholes, disk-hole coupling nanostructures and metal-insulator-metal (MIM) structures are briefly discussed.

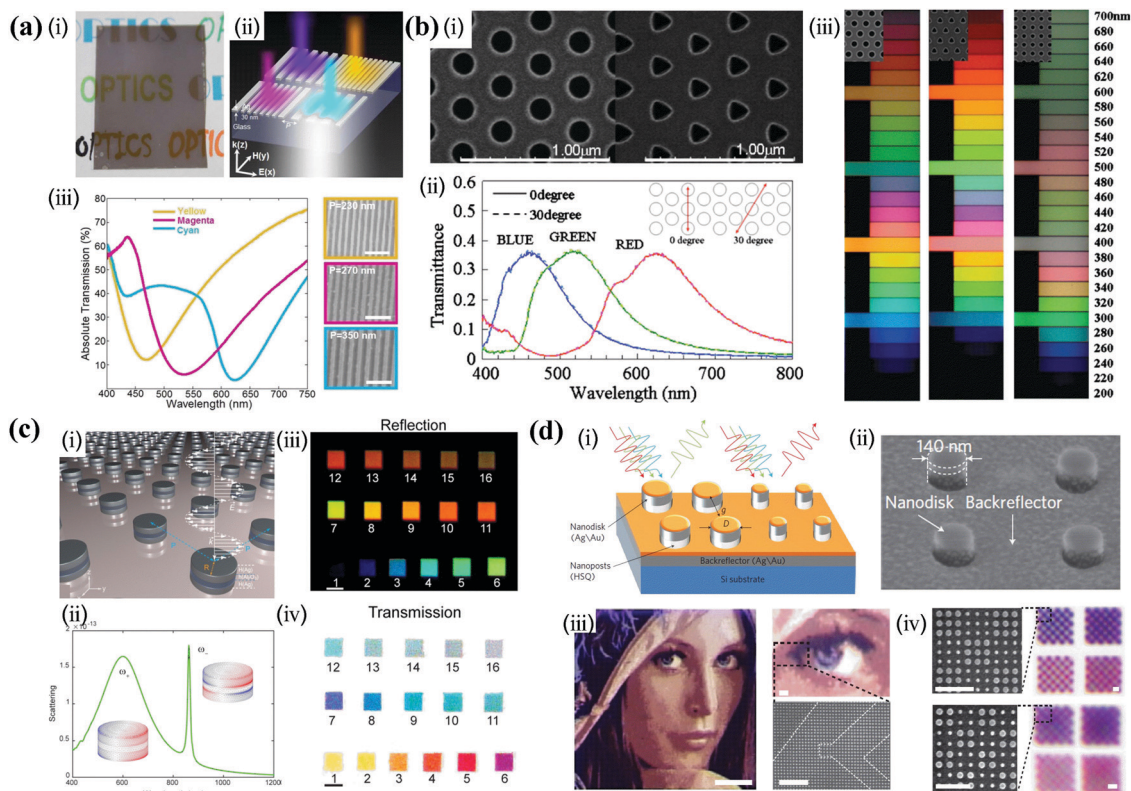


Fig. 2 Structural colors generated by plasmonic resonance. (a)(i)–(iii) a(i) Photo of a plasmonic nanograting consisting of 30 nm-thick Ag film deposited on glass slide, showing the word “OPTICS”. a(ii) Schematic diagram of the designed nanograting. a(iii) Measured transmission spectra of yellow, magenta and cyan grating with different periods. Insets show the corresponding SEM images of nanogratings. Reproduced from ref. 51, with permission from Nature Publishing Group, Copyright 2013. (b)(i)–(iii) b(i) SEM images of color filter composing Al nanoholes deposited on quartz substrate. b(ii) Measured transmission spectra of red, green and blue filters at 0° and 30° polarization angle. Insets show the corresponding top-view schematic of plasmonic nanoholes. b(iii) Optical microscope images of color filters with round holes and triangular holes on hexagonal lattice and round holes on square lattice. Reproduced from ref. 55, with permission from American Institute of Physics, Copyright 2011. (c)(i)–(iv) c(i) Schematic drawing of MIM tandem nanodisk array. Al_2O_3 layer is sandwiched between identical Ag layers in the unit cell. c(ii) Calculated scattering cross-section for a single MIM nanodisk. Insets shows the charge distribution of in-phase and out-of-phase modes, respectively. c(iii) and (iv) Measured colors palettes in (iii) transmission and (iv) reflection mode. Reproduced from ref. 61, with permission from American Chemical Society, Copyright 2017. (d)(i)–(iv) d(i) Schematic diagram and d(ii) SEM images of disk-hole coupling metasurface beyond optical diffraction limit. d(iii) Full-color printing image composing of disk-hole unit cells with distinct geometric sizes. Insets show the enlarged region and corresponding SEM image. d(iv) Resolution test pattern with array of 3×3 structures and 2×2 structures. Reproduced from ref. 66, with permission from Nature Publishing Group, Copyright 2012.

In its infancy, the study of plasmonic colors mainly concentrated on the transmission mode of the resonant spectra. Extraordinary optical transmission (EOT)⁴⁶ based on SP in an optically-thick opaque film can filter light at a specific resonant wavelength and lead to additive colors. In contrast, the counter-intuitive extraordinary low transmission (ELT) phenomenon,⁵⁰ realized by optically-thin semi-transparent metallic nanostructures, can selectively eliminate light at the resonant wavelength to generate subtractive colors. As shown in Fig. 2a(ii), a subtractive color filter based on 30 nm Ag nanograting was designed to generate yellow, magenta and cyan with high efficiency (Fig. 2a(iii)).⁵¹ In the nanoslits, the hybridization between localized surface plasmon polaritons (LSPPs) and short-range surface plasmon polaritons (SRSPs) leads to ELT resonance. Transmission minima can be arbitrarily tuned *via* varying geometric parameters across the entire visible range to control the colors. The pixel sizes of the nanograting are smaller than the commercial image sensors with the smallest pixels, which means that the plasmonic colors have

higher resolutions. However, owing to the polarization sensitivity, the one-dimensional (1D) nanostructures are limited in use in imaging or sensing applications.^{42,43,52,53} To implement polarization-independent colors, 2D symmetrical nanostructures on a homogeneous substrate are proposed; for example, the color filter in ref. 51, where high-quality subtractive colors were realized by ultra-thin nanopatches under arbitrary polarization angles.⁵⁴ Besides subtractive colors for printing, additive colors with a huge range are also important for displays and monitors. In Fig. 2b, additive colors in the transmission mode were realized by Al nanoholes on a quartz substrate.⁵⁵ Compared with high-cost Au and oxidizing Ag materials, Al with an interband transition lying outside the visible range enables stronger resonance, lower cost and higher tolerance to fabrication. The periodic metallic hole array can support the momentum to convert incident light into SP modes, and lead to an EOT effect. The micrographs in Fig. 2b(iii) record the wide range that nanoholes can achieve.

In addition, plasmonic colors can be achieved in a reflection mode based on specific nanostructures and mechanisms, such as MIM structures. Generally speaking, MIM nanostructures composed of a thin dielectric layer between the metal nano-antennas and the metal film can exhibit strong standing-wave resonance where the incident light is confined into the metallic gap.^{56–61} The weak interaction between adjacent unit cells results in encoding color into an individual nanoantenna. A single reflected peak can be formed to contribute to slightly higher saturation and a full hue of colors. Nevertheless, there is still a need to pursue higher-saturation colors performed by reflection spectra with a narrower peak. In this context, another MIM nanostructure is proposed to generate full colors in Fig. 2c.⁶¹ As shown in the schematic presented in Fig. 2c(i), a dielectric Al_2O_3 nanodisk is sandwiched by metallic Ag layers, which can be regarded as MIM structures. The scattering cross-section spectra of a single nanodisk has two hybridized plasmonic resonances, at high frequency ω_+ and low frequency ω_- . The corresponding charge distribution is shown in Fig. 2c(ii), implying the magnetic field between adjacent nanodisks is enhanced. The hybridization between Wood's anomaly and the in-phase electric mode gives rise to a narrower peak with high efficiency in the reflection mode and a lower valley in the transmission mode. As shown in Fig. 2c(iii), additive primary colors with higher saturation and brightness in the reflected field and subtractive primary colors (CMYK) in the transmissive field can be simultaneously generated by using MIM sandwich nanostructures.

Besides color saturation and hue, resolution is another crucial property for plasmonic structural colors in practical applications. As mentioned above, the pixels of nanodisks, nanoholes and gratings are approaching wavelength scale. In order to further improve resolution, disk-hole coupling nanostructures^{62–66} are introduced in Fig. 2(d).⁶⁶ Each pixel consists of four nanodisks, where Ag disks and the Au capping layers are raised above equally sized nanoholes on a backreflector (Fig. 2d(i and ii)). The Fano resonance resulting from the interference between the sharp resonance of the surface mode and the broad resonance of the nanodisk–nanohole coupling can lead to dips in the reflection spectra. Incident light flows around the nanodisks, through the nanoholes, and is absorbed by the backreflector. The interaction between Fano resonance and SP enables performing colors in a bright field. Furthermore, the resolution of pixels arranged in 250×250 nm units can reach 100 000 dpi. The resolution test pattern in Fig. 2d(iv) specifically shows the high resolution that the coupling nanostructures can reach. When the size of pixels is reduced to 250 nm, all colors in the chequerboard are preserved well, implying the resolution is approaching the optical diffraction limit.

Overall, high-quality structural colors both in reflection and transmission modes have been extensively generated by a variety of plasmonic metasurfaces.^{67–78} Compared with chemical pigments and dyes, plasmonic colors are preferable in terms of environment protection, high resolution, good durability, high flexibility and ease of fabrication. However, there are still drawbacks in plasmonic colors. The intrinsic ohmic loss resulting from free-electron scattering in metals leads to low efficiency and

broad resonant peaks in the reflection spectra. This means that there is still huge potential to improve the saturation of the three primary colors.

2.2 Colors from all-dielectric metasurfaces

To tackle the limits of high loss in plasmonic structures, all-dielectric metasurfaces with a high refractive index and low loss have been proposed as candidates. The dielectric nanostructures that interact with electromagnetic waves by a displacement current can support not only electric-dipole resonance, but also a comparable magnetic-dipole resonance.⁷⁹ Hence, all-dielectric metasurfaces, especially amorphous silicon (a-Si) nanostructures, have been extensively used to realize a range of phenomenal effects and functionalities in recent years. For instance, a magnetic reflector,⁸⁰ Huygens' effect,⁸¹ high-Q Fano resonance⁸² and wave-front control⁸³ have been demonstrated in the infrared range. However, in the visible wavelength, dielectric color filters have been shown to be challenging due to the convenient dielectric materials with either high loss (such as a-Si) or relatively low refractive index (such as Si_3N_4 and SiO_2).^{84,85} To address this limitation, some skillfully designed all-dielectric metasurfaces with highly saturated colors have been proposed. In the following section, we will systematically discuss high-quality dielectric color filters.

For a-Si color filter, there are invariably two aspects limiting the saturation and range of structural colors, which are high loss and substrate effect.⁸² That is, compared with the presence of the substrate, nanostructures can exhibit narrower spectra transitions from zero backward to suppressed forward scattering in free space. Therefore, an Si color filter can perform improved saturation of structural colors by suppressing the substrate effect or reducing material loss. On one hand, as shown in Fig. 3a, a 70 nm-thick Si_3N_4 membrane as an antireflective layer was coated over the silicon substrate.⁸⁶ The antireflective layer can create a substrateless environment that effectively suspends the Si nano-disks in free space. A direct correlation between the observed reflection and the particles' backscattering associated with Kerker's conditions^{87,88} is established based on the Si_3N_4 index matching layer. The multipolar decomposition in Fig. 3a(iii) indicates that the first Kerker's condition can be fully met in the dip at longer wavelengths, where reflection can be totally suppressed. The second Kerker's condition at shorter wavelengths is approximately satisfied since the phase difference is approximately π when the magnetic and electric modes hold the same amplitude. As a result, highly saturated colors generated from this metasurface are able to occupy about 120% standard RGB (sRGB) space by mimicking the Si nanostructure in free space in the reflection mode. The color printing in Fig. 3a(iv) intuitively exhibits full-hue and high-saturation colors. On the other hand, reducing loss of a-Si in the visible range is another way to improve the quality of the colors. In this context, hydrogenated amorphous silicon (a-Si:H), which is obtained *via* thermal annealing a-Si, has a lower extinction coefficient under the premise of maintaining a high refractive index.^{89,90} Compared with polycrystalline silicon (p-Si) with comparable loss, a-Si:H nanostructures have the advantages of low cost,

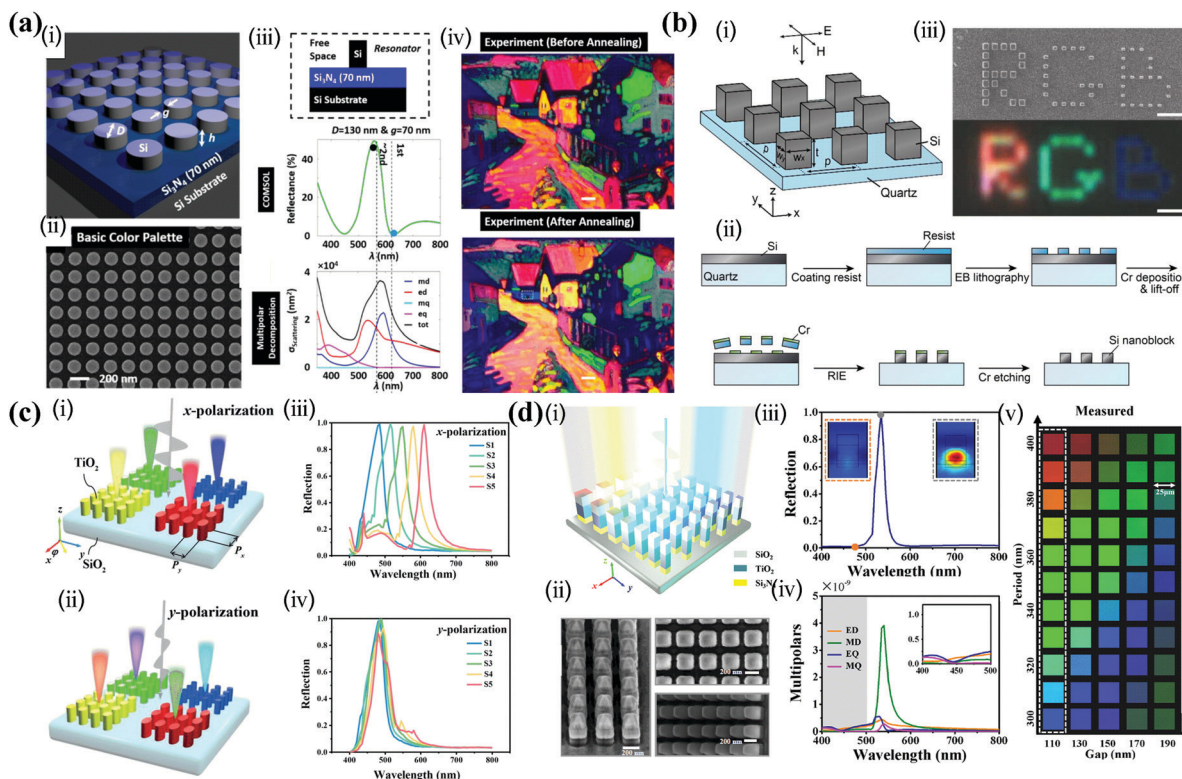


Fig. 3 Structural colors generated from all-dielectric metasurface. (a(i)–(iv)) a(i) Schematic and a(ii) SEM image of all-dielectric nanostructures consisting of amorphous Si nanodisks on 70 nm Si₃N₄ layer and SiO₂ substrate to mimicking free space. a(iii) Reflection spectra and multipolar decomposition of scattering cross-section when the diameter and gap size is 130 nm and 70 nm, respectively. a(iv) Color printing pictures before and after annealing. Reproduced from ref. 86, with permission from American Chemical Society, Copyright 2017. (b(i)–(iii)) b(i) Structural geometry of monocrystalline silicon nanostructures over silica substrate. b(ii) Fabricated process flow chart of the all-dielectric metasurface. b(iii) SEM image and measured image of letters “RGB” with three primary colors, respectively. Reproduced from ref. 94, with permission from American Chemical Society, Copyright 2017. (c(i)–(iv)) Schematic diagram of TiO₂ nanopillars arranged in distinct varying periods P_x and P_y under c(i) x and c(ii) y polarization states, respectively. Reflection spectra under c(iii) x and c(iv) y polarization states with varying size of P_x when P_y is fixed. Reproduced from ref. 98, with permission from Wiley-VCH Verlag GmbH & Co. KGaA, Weinheim, Copyright 2018. (d(i)–(v)) d(i) Configuration and d(ii) SEM image of multi-dielectric nanostructures resorting to stacked SiO₂, TiO₂ and Si₃N₄ nanodisks in reflection mode. d(iii) Reflection spectra and d(iv) multipolar decomposition of scattering cross-section of designed structure. The insets present magnetic field profile. d(v) Measured colors generated from all-dielectric nanostructures with changing gap and period. Reproduced from ref. 105, with permission from American Chemical Society, Copyright 2019.

efficient growth on substrates at relatively low temperatures and compatibility with the complementary metal oxide semiconductor (CMOS) process.^{90,91} Recently, three primary subtractive colors (CMY) with nearly 100% efficiency have been generated by all-dielectric metasurfaces incorporating a-Si:H nanodisks in transmission mode.⁹¹

Besides a-Si and p-Si, monocrystalline silicon (c-Si) has lower loss in the visible wavelength. When the wavelength is fixed at 410 nm, the extinction coefficients for a-Si, p-Si and c-Si are 2.02, 0.752 and 0.269, respectively, implying c-Si is a kind of ideal material for color filters.⁹² Nonetheless, the c-Si nanostructure is difficult to fabricate due to the incompatibility with the CMOS process.^{84,93} Recently, this challenge has been addressed by utilizing electron beam lithography (EBL) to fabricate the c-Si sample. As shown in the fabricated process of c-Si nanoblocks presented in Fig. 3b(ii), 150 nm-thick chemical resist is spin coated on a c-Si layer on a silica substrate. A 30 nm-thick Cr hard mask is deposited by a resist lift-off process after the designed patterns are drawn by EBL. Finally, the Cr mask is removed by immersing in a Cr

etching solution.⁹⁴ By using the fabricated c-Si nanoblocks, various brilliant structural colors are realized *via* tuning of the geometric parameters. Moreover, due to the high refractive index of c-Si, the pixels composed of a single nanoblock can present high-quality three primary colors in Fig. 3b(iii), indicating that this all-dielectric metasurface processes high resolution of about 85 000 dpi.

Although a variety of Si metasurfaces have realized highly saturated colors, the invariably existing loss in Si materials still hampers higher saturation and higher efficiency. As a result, TiO₂ as an alternative dielectric material with negligible loss in the visible range is a superior substitute to improve the purity of structural colors. To date, TiO₂ nanostructures with a large aspect ratio have been successfully fabricated by atomic layer deposition or electron beam evaporation.^{95–97} Due to the fact that the refractive index of TiO₂ is lower than in Si materials, a periodic arranging array of TiO₂ unit cells can be an effective way to enhance Mie resonances. The coupling between photonic crystal radiation and electric dipole resonances will significantly increase efficiency and reduce the bandwidth of the reflected peak;

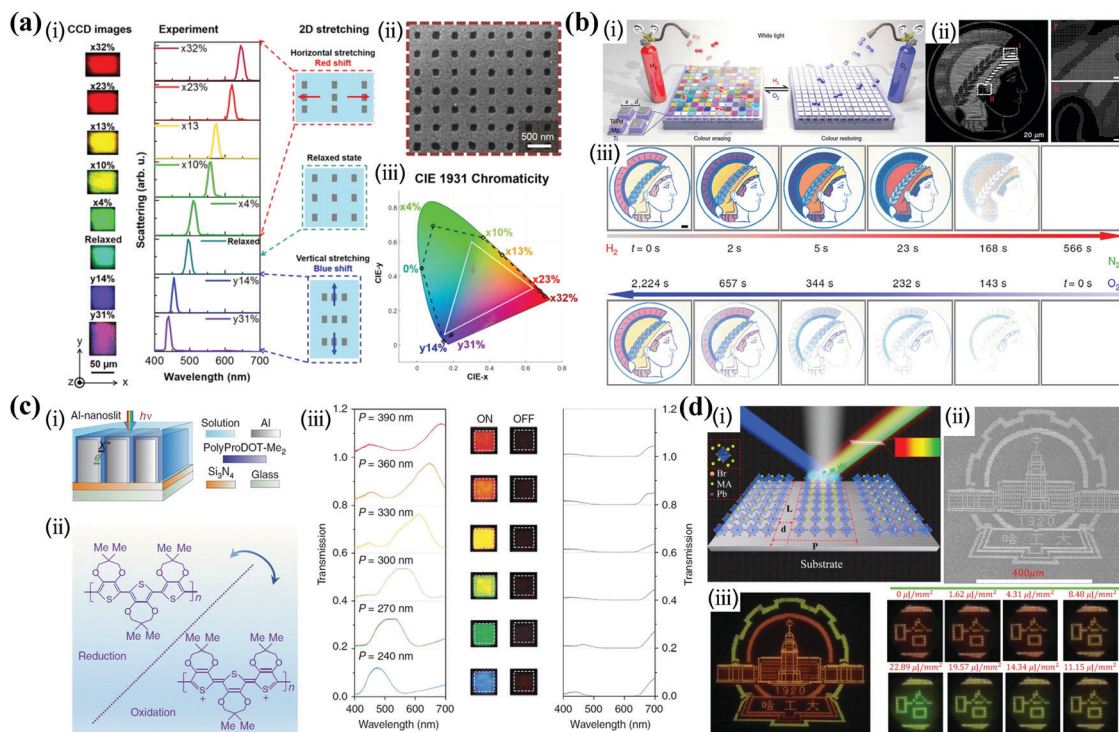


Fig. 4 Dynamically tunable structural colors (a(i)–(iii)) a(i) CCD images and measured scattering spectra of Al plasmonic array at different stretching conditions. a(ii) SEM image of the Al-coated Si template at relaxed state. a(iii) Full-color tuning in 1931 CIE chromaticity diagram with different stretching ratios. Reproduced from ref. 118, with permission from American Chemical Society, Copyright 2017. (b(i)–(iii)) b(i) Schematic diagram of plasmonic metasurface consisting of hydrogen-responsive Mg nanoblocks sandwiched between a Ti adhesion layer and Ti/Pd capping layers. The structural colors can be erased by hydrogen exposure and restored by oxygen exposure. b(ii) SEM images of the printing picture of Minerva logo. b(iii) Measured optical images by microscope during the process of hydrogenation and dehydrogenation to erasing and restoring colors, respectively. Reproduced from ref. 121, with permission from Nature Publishing Group, Copyright 2017. (c(i)–(iii)) c(i) Schematic of plasmonic electrochromic electrode composed of Al-nanoslit array. c(ii) Chemical structures of PolyProDOT-Me₂ in the oxidized and reduced form. c(iii) Measured transmission spectra of PolyProDOT-Me₂-coated Al-nanoslit metasurface for ON and OFF states of the polymer. Insets show corresponding color micrographs with increasing periods. Reproduced from ref. 129, with permission from Nature Publishing Group, Copyright 2016. (d(i)–(iii)) d(i) The schematic design of lead halide perovskite nanostructures color generation by mixing extrinsic structural color and intrinsic emission color. d(ii) Top-view SEM image of the logo. d(iii) Dynamic color printing by MAPbBr₃ meta-grating at different pumping density. Reproduced from ref. 132, with permission from American Chemical Society, Copyright 2018.

in other words, saturation of visible colors can be improved dramatically. For example, Fig. 3c shows a highly saturated color filter in reflection mode with nearly 100% efficiency based on TiO₂ nanopillars.⁹⁵ Fano resonance resulting from interference between the radiation waves of Mie resonance and directly reflected waves enables the generation of narrow-band spectra. In addition, the designed strategy of dependently varying periods along the *x* and *y* directions is utilized to simultaneously tune saturation and hue. By changing the polarization angle from 0° to 90°, three primary colors (RGB) with high saturation can be flexibly transformed, indicating that this color filter is anticipated to be applied in high-density optical data storage, hyperspectral microscopy and security encryption, for example.

Except for the all-dielectric nanostructures mentioned above, Si₃N₄ guided-mode resonant grating,^{99,100} perovskite nanostructures^{101,102} and SiGe resonator^{103,104} have also been studied for structural colors in recent years. In particular, a kind of multi-dielectric nanostructure consisting of stacked SiO₂, TiO₂ and Si₃N₄ layers is proposed to realize ultra-highly saturated colors, as shown in Fig. 3d.¹⁰⁵ The index matching of SiO₂ capping layer between TiO₂ layer and air, and Si₃N₄

bottom layer between silica substrate and TiO₂ layer can significantly suppress higher order modes at shorter wavelengths, and further improve the monochromaticity of the reflection spectra (Fig. 3d(iii and iv)). More than 85% energy of reflected light is confined in reflected colors. Based on this novel design, 171% sRGB space and 127% Adobe RGB space are taken up in the 1931 CIE chromaticity diagram, which is the largest color space generated from nanostructures as far as we know.

In summary, structural colors generated from all-dielectric metasurfaces offer high saturation and high efficiency, which can be extensively used in high-end displays and imaging applications.^{86,97,98,105} However, additive colors in the transmission mode are still rarely used within all-dielectric nanostructures. The urgent need now is to realize high-quality additive colors in transmission spectra.

3. Dynamically tunable structural colors

Having dynamically tunable colors *in situ* is essential for advanced displays with novel functionalities, such as color printing,

animations and security encryption. However, the tuning of most structural colors generated from plasmonic and dielectric metasurfaces is dependent on changing physical parameters, which is difficult in fabricated processes.^{106,107} To overcome this limitation, several methods have been used to realize dynamic tuning.^{108–110} For instance, changing the relative orientations of resonators to tune different resonant modes, or using phase-change materials, voltage-control coupling and thermal stimulus to tune metasurfaces.^{111–113} Here, four tunable methods of mechanical stretching, chemical reaction, electrical control and photon doping are reviewed.

Mechanical stretching is the most common way to realize dynamic tuning of near-field interaction *via* varying period of lattice. In stretched technologies, polydimethylsiloxane (PDMS), as an elastomeric matrix, holds the advantages of elasticity, inertia, nontoxicity and nonflammability.^{109,114} In recent years, mechanically stretched devices have been widely used in interactive LEDs,¹¹⁵ solar cells¹¹⁶ and tunable metalens.¹¹⁷ In particular, the full-color tunable filter by means of mechanical stretching is proposed across the entire visible range, as presented in Fig. 4a.¹¹⁸ Al nanostructures with high bulk plasma frequency from the ultraviolet to infrared range are patterned over the PDMS substrate *via* the EBL process. The scattering spectra depending on the excitation and restricted collection angles is highly sensitive to the period of lattice. As a result, when the nanostructure is designed to perform green in the relaxed state, the scattering spectra will red shift and blue shift in the state of stretching along the *x* and *y* axes, respectively (Fig. 4a(i)). The mechanically stretched filter is an ideal device to integrate into a micro-electromechanical system (MEMS), such as ultracompact MEMS-based spectrometers.

Chemical transition is another way to realize dynamic tuning of structural colors; namely, tuning resonance *via* changing components of nanostructures, where Mg material with superior plasmonic properties is a perfect choice in the visible wavelength.^{119,120} In the field of solid-state hydrogen storage, Mg is one of the most promising candidates, because up to 7.6 wt% of hydrogen gas can be absorbed.¹¹⁹ Therefore, metallic-state Mg and dielectric-state MgH₂ are able to undergo chemical transition *via* the processes of hydrogenation and dehydrogenation, respectively. Based on this unique property of catalytic Mg, Fig. 4b shows a dynamic color filter comprising an Mg layer sandwiched between Ti/Pd capping layers and a Ti adhesion layer.¹²¹ Upon hydrogen exposure, Mg nanoparticles will go through a series of complicated chemical processes, and the fraction of metal Mg will gradually decrease, rendering a dynamic change from plasmonic colors to dielectric colors. Due to the fact that the Mie resonances of MgH₂ nanoparticles are weak in the visible range, the colors can be erased after hydrogenation. More importantly, the erased process is reversible through dehydrogenation in the presence of oxygen (Fig. 4b(iii)). The flexible colors are promising to be used in dynamic color displays with functionalities of tunable colors, encryption and animations.

Besides physical and chemical tuning, electronic control is also a good way to tune colors due to ultra-thin, low-power-consuming and flexible merits.^{122,123} In electronic technology, the phase transition from the nematic to the isotropic state of

liquid crystals (LC) can be used to tune resonance under an applied voltage.^{108,124,125} However, the high cost, lack of bistability and complicated fabrication of LC nanostructures still remain a challenge. Hence, several electrochromic materials, such as conducting polymers and transition metal oxides, have been utilized to dynamically tune colors.^{126–128} For instance, Fig. 4c illustrates full-color electrochromic switching by use of polyaniline (PANI) and poly(2,2-dimethyl-3,4-propylenedioxythiophene) (PolyProDOT-Me₂), which can both be conformally and controllable electrodeposited on Al nanoslits.¹²⁹ To further improve the purity of colors, an Si₃N₄ waveguide as a buffer layer is set underneath the Al nanoslits to narrow the linewidth of the spectra (Fig. 4c(i)). By applying different voltages, oxidized and reductive PolyProDOT-Me₂ with changing refractive indices will be switched, as shown in Fig. 4c(i), which means switching colors can be realized at ON and OFF states by using different voltages. The electrochromic switching with fast speed and high-contrast colors has promising applications, ranging from catalysis to photovoltaics.

Finally, photon doping can be used to realize dynamically tunable *in situ* structural colors. In addition to the extrinsic structural colors generated from light-matter interaction, the intrinsic emission colors caused by photoluminescence (PL) of the active materials is introduced in the photon-doping method.^{130,131} As shown in the schematic presented in Fig. 4d, methylammonium lead halide perovskite (MAPbBr₃, where MA = CH₃NH₃⁺) gratings are patterned on a glass substrate *via* a top-down process.¹³² MAPbBr₃ material as a semiconductor possesses intrinsic emissions generated from the direct bandgap. The intensity of the intrinsic emission colors can be determined by the excitation; that is, the density of the pumping laser. Hence, mixing of the extrinsic structural colors and intrinsic emission colors leads to a new color. Based on Grassmann's law, changing the intensity of intrinsic colors by use of a pumping laser enables the *in situ* new color to be dynamically tuned. The dynamic tuning is reversible with decreasing pumping intensity. More significantly, the color-transition time is mainly determined by buildup, and ring down time of PL is of the order of nanoseconds, which is orders of magnitude faster than previous studies. The enlarged measured printing in Fig. 4d(iii) shows flexibly dynamic tuning from red to green by changing the intensity of pumping light.

4. Applications

As shown in the previous sections, static and dynamic structural colors have been widely realized in metasurfaces. Because of the ultra-thin, ultracompact, highly durable and environmentally benign properties of the nanostructures, the full-color filters with high saturation, high efficiency and high resolution are promising alternatives to replace conventional pigments in many practical applications. In the following section, displays, encryption and sensing applications based on structural colors are introduced.

To date, high-end and advanced displays have attracted the most attention in the study of structural colors. In Fig. 5a, a

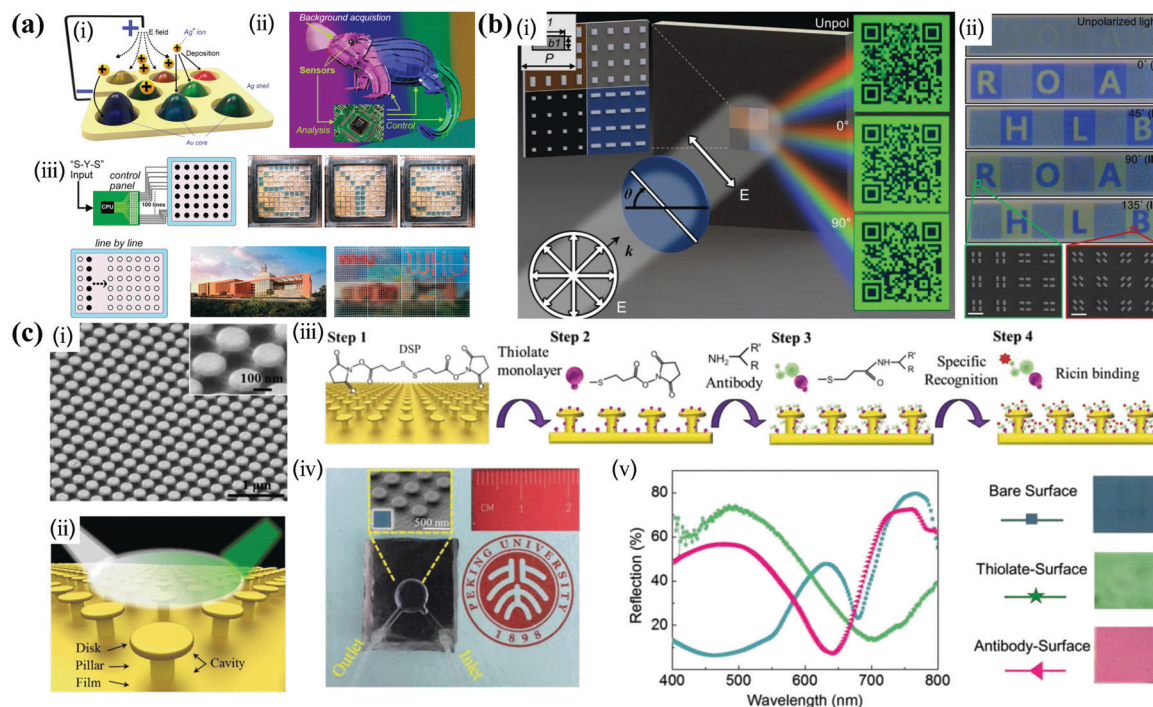


Fig. 5 Practical applications of structural colors generated from metasurface. (a)(i)–(iii) a(i) Schematic of designed plasmonic cell composed of nanodomes with different Ag shell thickness. a(ii) Schematic diagram of the plastic chameleon covered with plasmonic cells. a(iii) Operational schematic and screenshots of fast display and static display, which consist of designed plasmonic cells. Reproduced from ref. 133, with permission from American Chemical Society, Copyright 2016. (b)(i)–(ii) b(i) Schematic of Kerker-conditioned cryptographic nanostructures composed of a-Si:H nanoblocks over silica substrate. Different information can be decoded in a predetermined polarization angle. b(ii) Measured optical images of the encrypted “RHOLAB” message which can be decoded by polarized light at specific angle. Reproduced from ref. 134, with permission from Wiley-VCH Verlag GmbH & Co. KGaA, Weinheim, Copyright 2018. (c)(i)–(v) c(i) SEM image and c(ii) Schematic diagram of nanopin-cavity resonator for quantitative colorimetric ricin sensing. c(iii) Schematic of antibody immobilization on nanopins metasurface for ricin visual detection. c(iv) Bright-field micrograph of microfluidic channel device. Insets show enlarged SEM image of nanopins array and their color appearance. c(v) Spectra shift and colors variation of biofunctionalized procedure due to the inter-molecular interaction. Reproduced from ref. 139, with permission from Wiley-VCH Verlag GmbH & Co. KGaA, Weinheim, Copyright 2016.

dynamic plasmonic nanostructure based on Au/Ag nanodomes is integrated into a designed matrix display covering the entire visible range.¹³³ The method of electrodeposition can be utilized to dynamically alter the thickness of Ag shells on Au nanodomes by applying a voltage, and rendering a continuous color change based on a reversible redox reaction of Ag. During the process of redox, the colors will gradually change with the time of the oxidation/reduction reaction, which is consistent with the cyclic voltammogram measurement. In the design of a biomimetic chameleon (Fig. 5b(ii)), the chameleon covered with plasmonic nanodomes is equipped with color sensors to sense the environment's color. And then the color information is automatically analyzed and delivered into the nanodomes so as to change the color of the chameleon accordingly. This implies that optical wearable devices are possible. In Fig. 5a(iii), rapid display with the responsive speed of a unit cell and static display, where the unit cells are operated by a line-by-line matrix-addressing technique, are respectively demonstrated, showing the potential of high-end displays and imaging applications.

Fig. 5b shows a dynamic cryptographic nanostructure based on asymmetric a-Si:H nanoantennas on a silica substrate.¹³⁴ By means of meticulously designing geometric parameters,

Kerker's conditions can be fully met, and lead to a narrowed resonant peak and suppression of unwanted light; that is, improved saturation of structural colors. More importantly, the polarization-dependent property resulting from the asymmetric structures gives rise to the possibility of storing different optical information in distinct polarization states. As presented in Fig. 5b(i), a fixed nanostructure shows different quickmark codes in 0° and 90° polarization angles. Hence, the nanostructure can be a possible design strategy to realize cryptographic nanoprints *via* controlling polarization angles, such as the test of cryptograph shown in Fig. 5b(ii). Four kinds of pixel with 0° and 90° rotated angles for “R, O, A” and 45° and 135° rotated angles for “H, L, B” are used to encrypt information in designated polarization angles. These cryptographic nanoprints can be compatible with a smartphone, security tag, payment, identification and anti-counterfeiting.

Moreover, colorimetric sensing based on plasmonic structural colors has been introduced to detect analytes by directly observing changes of visible colors.^{42,135–138} However, the broad resonant spectra caused by localized surface plasmon resonance (LSPR) generally leads to reduced colorimetric resolution due to the strong radiative damping. For example, the highest LSPR sensitivity of an Au sensor is focused on the near-infrared range. To overcome the

limitation of LSPR sensing, a skillfully designed strategy is used to improve colorimetric capacity. For instance, 2D Al nanoclusters have been designed to provide Fano resonance with energies in the region from blue to green, which is the most sensitive part for human eyes.¹³⁸ The detected colors can gradually change from blue to orange when the analytes are air ($n = 1.0$), PDMS ($n = 1.4$), poly(methyl methacrylate) (PMMA) ($n = 1.5$) and diphenyl ether ($n = 1.6$), respectively. Furthermore, in the field of biosensing, quantitative colorimetric sensing of ricin is also reached in Fig. 5c based on nanopin-cavity resonator,¹³⁹ by which bright-field structural colors are fully realized (Fig. 5c(ii)). The location of the resonant peak in the visible range can be flexibly tuned by changing the medium indices. As presented in Fig. 5c(iii), an antibody-functionalized biosensor with high sensitivity and fast response is fabricated to detect ricin. The antibody protein can be immobilized by use of the amide linkage formed by the reaction of the terminal succinimide group with the amine of protein. Based on the biosensor, the density of ricin can be observed by a dramatic color change at less than 10 min.

5. Summary and prospects

We have reviewed the development of structural colors based on plasmonic and dielectric metasurfaces to date. The plasmonic additive and subtractive colors caused by SPP resonance have been widely realized *via* nanogratings, nanoholes, disk-hole coupling and MIM nanostructures in both transmission and reflection modes. Although the inherent loss of metal materials hinders higher saturation and efficiency, remarkably high resolution approaching 100 000 dpi is possible by use of disk-hole coupling. While for dielectric colors, Mie resonances generated from high-index dielectric nanostructures lead to high-quality reflection spectra with narrow linewidth and high efficiency; namely highly saturated colors. Significantly, a multi-dielectric metasurface based on multipolar modulation has recently obtained a huge color space occupied 171% sRGB space. However, there is still the challenge of realizing additive colors in the transmission mode within all-dielectric metasurfaces. Based on these color filters, a number of methods of dynamically tunable colors, including mechanical stretching, chemical reaction, electrical control and photon doping, are systematically discussed in this paper. The ultra-thin thickness of the color filters has the potential to integrate on a chip, indicating that structural colors generated from metasurfaces are promising in terms of a new paradigm for practical applications; for example, biosensing, colorimetric sensing, high-end displays, encryption, anti-counterfeiting, high-density optical data storage, holograms and so on. In summary, there is great significance and enormous potential application in the study of structural colors.

However, looking ahead, there are still obstacles that need to be addressed in the development of practical color filters. First of all, high-quality additive colors with both high saturation and high resolution are rare in the transmission mode, which is of significant importance for holograms and advanced imaging applications. In addition, color filters need to be combined with practical applications as much as possible. Mass production is

still a challenge since Ag and Au are too expensive within plasmonic nanostructures, and TiO₂ and c-Si are not compatible with CMOS process within dielectric nanostructures. Although Al or a-Si seem to be good choices for practical production, high loss invariably hampers the generation of highly saturated colors. That means new designed strategies and fabricated technologies are imminently required in the subsequent research. For instance, hybridization between dielectric and plasmonic materials can be a promising platform for additive structural colors in the transmission mode by meticulous design. On the other hand, possible approaches in terms of nanoimprint lithography, self-assembly technique and injection molding need to be developed in practice to realize mass production. Overall, there is still huge space to be explored in relation to structural colors before commercialization. We believe colors generated from metasurfaces can be extensively used to take the place of chemical pigments, and dramatically improve the quality of our daily life in the future.

Conflicts of interest

There are no conflicts to declare.

Acknowledgements

This work was supported by the National Key Research and Development Program of China (2016YFA0301102 and 2017YFA0303800), the National Natural Science Foundation of China (91856101, 11574163, and 11774186), Natural Science Foundation of Tianjin for Distinguished Young Scientists (18JCQJC45700), the Natural Science Foundation of Tianjin (16JCQNJC01700), and 111 Project (B07013).

Notes and references

- O. Meth-Cohn and M. Smith, *J. Chem. Soc., Perkin Trans. 1*, 1994, 5–7.
- D. D. Oprian, A. B. Asenjo, N. Lee and S. L. Pelletier, *Biochemistry*, 1991, **30**, 11367–11372.
- A. J. Melendez-Martinez, G. Britton, I. M. Vicario and F. J. Heredia, *Food Chem.*, 2007, **101**, 1145–1150.
- Z. Hao and A. Iqbal, *Chem. Soc. Rev.*, 1997, **26**, 203–213.
- W. Yue, S. Gao, S.-S. Lee, E.-S. Kim and D.-Y. Choi, *Laser Photonics Rev.*, 2017, **11**, 1600285.
- Y. Wang, M. Zheng, Q. Ruan, Y. Zhou, Y. Chen, P. Dai, Z. Yang, Z. Lin, Y. Long, Y. Li, N. Liu, C.-W. Qiu, J. K. W. Yang and H. Duan, *Research*, 2018, 8109054.
- H. Ghiradella, *Appl. Opt.*, 1991, **30**, 3492–3500.
- S. Kinoshita, S. Yoshioka and J. Miyazaki, *Rep. Prog. Phys.*, 2008, **71**, 076401.
- Y. Fu, C. A. Tippetts, E. U. Donev and R. Lopez, *Wiley Interdiscip. Rev.: Nanomed. Nanobiotechnol.*, 2016, **8**, 758–775.
- K. Zhang, Y. Tang, J. Meng, G. Wang, H. Zhou, T. Fan and D. Zhang, *Opt. Express*, 2014, **22**, 27437–27450.
- N. Okada, D. Zhu, D. Cai, J. B. Cole, M. Kambe and S. Kinoshita, *J. Opt.*, 2013, **42**, 25–36.

- 12 Y. Shen, V. Rinnerbauer, I. Wang, V. Stelmakh, J. D. Joannopoulos and M. Soljacic, *ACS Photonics*, 2015, **2**, 27–32.
- 13 F. Cheng, J. Gao, T. S. Luk and X. Yang, *Sci. Rep.*, 2015, **5**, 11045.
- 14 J. S. Clausen, E. Højlund-Nielsen, A. B. Christiansen, S. Yazdi, M. Grajower, H. Taha, U. Levy, A. Kristensen and N. A. Mortensen, *Nano Lett.*, 2014, **14**, 4499–4504.
- 15 T. Xu, H. Shi, Y.-K. Wu, A. F. Kaplan, J. G. Ok and L. J. Guo, *Small*, 2011, **7**, 3128–3136.
- 16 Y. Gu, L. Zhang, J. K. W. Yang, S. P. Yeo and C.-W. Qiu, *Nanoscale*, 2015, **7**, 6409.
- 17 P. Genevet, F. Capasso, F. Aieta, M. Khorasaninejad and R. Devlin, *Optica*, 2017, **4**, 139–152.
- 18 E. Karimi, S. A. Schulz, I. D. Leon, H. Qassim, J. Upham and R. W. Boyd, *Light: Sci. Appl.*, 2014, **3**, e167.
- 19 N. Meinzer, W. L. Barnes and L. R. Hooper, *Nat. Photonics*, 2014, **8**, 889.
- 20 J. Wang and J. Du, *Appl. Sci.*, 2016, **6**, 239.
- 21 A. Krasnok, S. Makarov, M. Petrov, R. Savelev, P. Belov and Y. Kivshar, *SPIE Opt. Optoelectr.*, 2015, **9502**, 950203.
- 22 M. I. Shalae, J. Sun, A. Tsukernik, A. Pandey, K. Nikolskiy and N. M. Litchinitser, *Nano Lett.*, 2015, **15**, 6261–6266.
- 23 A. I. Kuznetsov, A. E. Miroshnichenko, M. L. Brongersma, Y. S. Kivshar and B. Luk'yanchuk, *Science*, 2016, **354**, aag2472.
- 24 X. Yin, Z. Ye, J. Rho, Y. Wang and X. Zhang, *Science*, 2013, **339**, 1405–1407.
- 25 Z. Li, W. Liu, H. Cheng, S. Chen and J. Tian, *Adv. Opt. Mater.*, 2017, **5**, 1700413.
- 26 Z. Li, W. Liu, H. Cheng, J. Liu, S. Chen and J. Tian, *Sci. Rep.*, 2016, **6**, 35485.
- 27 Z. Li, W. Liu, H. Cheng, S. Chen and J. Tian, *Opt. Lett.*, 2016, **41**, 3142–3145.
- 28 J. Lee, M. Tymchenko, C. Argyropoulos, P.-Y. Chen, F. Lu, F. Demmerle, G. Boehm, M.-C. Amann, A. Alù and M. A. Belkin, *Nature*, 2014, **511**, 65.
- 29 Z. Li, W. Liu, Z. Li, H. Cheng, S. Chen and J. Tian, *Opt. Lett.*, 2017, **42**, 3117–3120.
- 30 Z. Li, W. Liu, Z. Li, H. Cheng, J. Li, X. Chen, S. Chen and J. Tian, *Laser Photonics Rev.*, 2018, **12**, 1800164.
- 31 A. V. Kildishev, A. Boltasseva and V. M. Shalae, *Science*, 2013, **339**, 1232009.
- 32 L. Huang, X. Chen, B. Bai, Q. Tan, G. Jin, T. Zentgraf and S. Zhang, *Light: Sci. Appl.*, 2013, **2**, e70.
- 33 S. Chen, Z. Li, W. Liu, H. Cheng and J. Tian, *Adv. Mater.*, 2019, 1802458.
- 34 L. Huang, X. Chen, H. Mühlenbernd, H. Zhang, S. Chen, B. Bai, Q. Tan, G. Jin, K.-W. Cheah, C.-W. Qiu, J. Li, T. Zentgraf and S. Zhang, *Nat. Commun.*, 2013, **4**, 2808.
- 35 G. Zheng, H. Mühlenbernd, M. Kenney, G. Li, T. Zentgraf and S. Zhang, *Nat. Nanotechnol.*, 2015, **10**, 308.
- 36 Z. Li, M.-H. Kim, C. Wang, Z. Han, S. Shrestha, A. C. Overvig, M. Lu, A. Stein, A. M. Agarwal, M. Lončar and N. Yu, *Nat. Nanotechnol.*, 2017, **12**, 675.
- 37 A. Pors, M. G. Nielsen, R. L. Eriksen and S. I. Bozhevolnyi, *Nano Lett.*, 2013, **13**, 829–834.
- 38 A. A. High, R. C. Devlin, A. Dibos, M. Polking, D. S. Wild, J. Perczel, N. P. de Leon, M. D. Lukin and H. Park, *Nature*, 2015, **522**, 192.
- 39 N. Yu, F. Aieta, P. Genevet, M. A. Kats, Z. Gaburro and F. Capasso, *Nano Lett.*, 2012, **12**, 6328–6333.
- 40 F. Ding, Z. Wang, S. He, V. M. Shalae and A. V. Kildishev, *ACS Nano*, 2015, **9**, 4111–4119.
- 41 Z. Li, A. W. Clark and J. M. Cooper, *ACS Nano*, 2016, **10**, 492–498.
- 42 M. Song, X. Li, M. Pu, Y. Guo, K. Liu, H. Yu, X. Ma and X. Luo, *Nanophotonics*, 2018, **7**, 323–331.
- 43 L. Duempelmann, A. Luu-Dinh, B. Gallinet and L. Novotny, *ACS Photonics*, 2016, **3**, 190–196.
- 44 X. M. Goh, Y. Zheng, S. J. Tan, L. Zhang, K. Kumar, C.-W. Qiu and J. K. W. Yang, *Nat. Commun.*, 2014, **5**, 5361.
- 45 J.-M. Guay, A. C. Lesina, G. Côté, M. Charron, D. Poitras, L. Ramunno, P. Berini and A. Weck, *Nat. Commun.*, 2017, **8**, 16095.
- 46 Q. Chen and D. R. S. Cumming, *Opt. Express*, 2010, **18**, 14056–14062.
- 47 F. Cheng, J. Gao, L. Stan, D. Rosenmann, D. Czaplewski and X. Yang, *Opt. Express*, 2015, **23**, 14552–14560.
- 48 F. Cheng, X. Yang, D. Rosenmann, L. Stan, D. Czaplewski and J. Gao, *Opt. Express*, 2015, **23**, 25329–25339.
- 49 W. Wang, D. Rosenmann, D. A. Czaplewski, X. Yang and J. Gao, *Opt. Express*, 2017, **25**, 20454–20465.
- 50 Z. Wei, Y. Cao, X. Su, Z. Gong, Y. Long and H. Li, *Opt. Express*, 2013, **21**, 10739–10745.
- 51 B. Zeng, Y. Gao and F. J. Bartoill, *Sci. Rep.*, 2013, **3**, 2840.
- 52 T. Xu, Y.-K. Wu, X. Luo and L. J. Guo, *Nat. Commun.*, 2010, **1**, 59.
- 53 H. J. Park, T. Xu, J. Y. Lee, A. Ledbetter and L. J. Guo, *ACS Nano*, 2011, **5**, 7055–7060.
- 54 H.-S. Lee, Y.-T. Yoon, S.-S. Lee, S.-H. Kim and K.-D. Lee, *Opt. Express*, 2007, **15**, 15457–15463.
- 55 D. Inoue, A. Miura, T. Nomura, H. Fujikawa, K. Sato, N. Ikeda, D. Tsuya, Y. Sugimoto and Y. Koide, *Appl. Phys. Lett.*, 2011, **98**, 093113.
- 56 M. Miyata, H. Hatada and J. Takahara, *Nano Lett.*, 2016, **16**, 3166–3172.
- 57 H. Kim, M. Kim, T. Chang, A. Baucour, S. Jeon, N. Kim, H.-J. Choi, H. Lee and J. Shin, *Opt. Express*, 2018, **26**, 27403–27417.
- 58 A. S. Roberts, A. P. Albreksten and S. I. Bozhevolnyi, *Nano Lett.*, 2014, **14**, 783–787.
- 59 C. Yang, W. Shen, Y. Zhang, H. Peng, X. Zhang and X. Liu, *Opt. Express*, 2014, **22**, 11384–11391.
- 60 Y. Ren, Y. Lu, T. Zang, Y. Wang, Y. Dai and P. Wang, *Opt. Express*, 2017, **25**, 28417–28426.
- 61 H. Wang, X. Wang, C. Yan, H. Zhao, J. Zhang, C. Santschi and O. J. F. Martin, *ACS Nano*, 2017, **11**, 4419–4427.
- 62 S. J. Tan, L. Zhang, D. Zhu, X. M. Goh, Y. M. Wang, K. Kumar, C.-W. Qiu and J. K. W. Yang, *Nano Lett.*, 2014, **14**, 4023–4029.
- 63 J. S. Clausen, E. Højlund-Nielsen, A. B. Christiansen, S. Yazdi, M. Grajower, H. Taha, U. Levy, A. Kristensen and N. A. Mortensen, *Nano Lett.*, 2014, **14**, 4499–4504.

- 64 X. Zhu, C. Vannahme, E. Højlund-Nielsen, N. A. Mortensen and A. Kristensen, *Nat. Nanotechnol.*, 2016, **11**, 325–329.
- 65 B.-R. Lu, C. Xu, J. Liao, J. Liu and Y. Chen, *Opt. Lett.*, 2016, **41**, 1400–1403.
- 66 K. Kumar, H. Duan, R. S. Hegde, S. C. W. Koh, J. N. Wei and J. K. W. Yang, *Nat. Nanotechnol.*, 2012, **7**, 557.
- 67 P. Mandal, S. A. Ramakrishna, R. Patil and A. V. Gopal, *Appl. Phys. Lett.*, 2013, **114**, 224303.
- 68 A. G. Nikitin, *Appl. Phys. Lett.*, 2016, **108**, 051112.
- 69 K.-T. Lee, S. Y. Han and H. J. Park, *Adv. Opt. Mater.*, 2017, **5**, 1700284.
- 70 L. Wang, R. J. H. Ng, S. S. Dinachali, M. Jalali, Y. Yu and J. K. W. Yang, *ACS Photonics*, 2016, **3**, 627–633.
- 71 R. Yu, P. Mazumder, N. F. Borrelli, A. Carrilero, D. S. Ghosh, R. A. Maniyara, D. Baker, F. J. G. de Abajo and V. Pruneri, *ACS Photonics*, 2016, **3**, 1194–1201.
- 72 X. M. Goh, R. J. H. Ng, S. Wang, S. J. Tan and J. K. W. Yang, *ACS Photonics*, 2016, **3**, 1000–1009.
- 73 R. J. H. Ng, X. M. Goh and J. K. W. Yang, *Opt. Express*, 2015, **23**, 32597–32605.
- 74 Z. Li, W. Wang, D. Rosenmann, D. A. Czuplewski, X. Yang and J. Gao, *Opt. Express*, 2016, **24**, 20472–20480.
- 75 M. Ye, L. Sun, X. Hu, B. Shi, B. Zeng, L. Wang, J. Zhao, S. Yang, R. Tai, H.-J. Fecht, J.-Z. Jiang and D.-X. Zhang, *Opt. Lett.*, 2015, **40**, 4979–4982.
- 76 Z. Li, S. Butun and K. Aydin, *ACS Photonics*, 2015, **2**, 183–188.
- 77 Y.-K. R. Wu, A. E. Hollowell, C. Zhang and L. J. Guo, *Sci. Rep.*, 2013, **3**, 1194.
- 78 J. Olson, A. Manjavacas, L. Liu, W.-S. Chang, B. Foerster, N. S. King, M. W. Knight, P. Nordlander, N. J. Halas and S. Link, *Proc. Natl. Acad. Sci. U. S. A.*, 2014, **111**, 14348–14353.
- 79 S. Jahani and Z. Jacob, *Nat. Nanotechnol.*, 2016, **11**, 23.
- 80 Z. Ma, S. M. Hanham, P. Albella, B. Ng, H. T. Lu, Y. Gong, S. A. Maier and M. Hong, *ACS Photonics*, 2016, **3**, 1010–1018.
- 81 M. Decker, I. Staude, M. Falkner, J. Dominguez, D. N. Neshev, I. Brener, T. Pertsch and Y. S. Kivshar, *Adv. Opt. Mater.*, 2015, **3**, 813–820.
- 82 C. Wu, N. Arju, G. Kelp, J. A. Fan, J. Dominguez, E. Gonzales, E. Tutuc, I. Brener and G. Shvets, *Nat. Commun.*, 2014, **5**, 3892.
- 83 K. E. Chong, I. Staude, A. James, J. Dominguez, S. Liu, S. Campione, G. S. Subramania, T. S. Luk, M. Decker, D. N. Neshev, I. Brener and Y. S. Kivshar, *Nano Lett.*, 2015, **15**, 5369–5374.
- 84 D. Sell, J. Yang, S. Doshay, K. Zhang and J. A. Fan, *ACS Photonics*, 2016, **3**, 1919–1925.
- 85 V. Vashistha, G. Vaidya, R. S. Hegde, A. F. Serebryannikov, N. Bonod and M. Krawczyk, *ACS Photonics*, 2017, **4**, 1076–1082.
- 86 Z. Dong, J. Ho, Y. F. Yu, Y. H. Fu, R. Paniagua-Dominguez, S. Wang, A. I. Kuznetsov and J. K. W. Yang, *Nano Lett.*, 2017, **17**, 7620–7628.
- 87 R. Alaee, R. Filter, D. Lehr, F. Lederer and C. Rockstuhl, *Opt. Lett.*, 2015, **40**, 2645–2648.
- 88 V. E. Babicheva and A. B. Evlyukhin, *Laser Photonics Rev.*, 2017, **11**, 1700132.
- 89 S. V. Makarov, A. N. Tsypkin, T. A. Voytova, V. A. Milichko, I. S. Mukhin, A. V. Yulin, S. E. Putilin, M. A. Baranov, A. E. Krasnok, I. A. Morozov and P. A. Belov, *Nanoscale*, 2016, **8**, 17809–17814.
- 90 I. Koirala, V. R. Shrestha, C.-S. Park, S. Gao, S.-S. Lee and D.-Y. Choi, *Sci. Rep.*, 2017, **7**, 2556.
- 91 C.-S. Park, V. R. Shrestha, W. Yue, S. Gao, S.-S. Lee, E.-S. Kim and D.-Y. Choi, *Sci. Rep.*, 2017, **7**, 2556.
- 92 E. D. Palik, *Handbook of optical constants of solids*, Academic Press, New York, 1991.
- 93 Z. Zhou, J. Li, R. Su, B. Yao, H. Fang, K. Li, L. Zhou, J. Liu, D. Stellinga, C. P. Reardon, T. F. Krauss and X. Wang, *ACS Photonics*, 2017, **4**, 544–551.
- 94 Y. Nagasaki, M. Suzuki and J. Takahara, *Nano Lett.*, 2017, **17**, 7500–7506.
- 95 J. P. B. Mueller, N. A. Rubin, R. C. Devlin, B. Groever and F. Capasso, *Phys. Rev. Lett.*, 2017, **118**, 113901.
- 96 M. Khorasaninejad, Z. Shi, A. Y. Zhu, W. T. Chen, V. Sanjeev, A. Zaidi and F. Capasso, *Nano Lett.*, 2017, **17**, 1819–1824.
- 97 S. Sun, Z. Zhou, C. Zhang, Y. Gao, Z. Duan, S. Xiao and Q. Song, *ACS Nano*, 2017, **11**, 4445–4452.
- 98 B. Yang, W. Liu, Z. Li, H. Cheng, S. Chen and J. Tian, *Adv. Opt. Mater.*, 2018, **6**, 1701009.
- 99 M. J. Uddin, T. Khaleque and R. Magnusson, *Opt. Express*, 2014, **22**, 12307–12315.
- 100 M. J. Uddin and R. Magnusson, *Opt. Express*, 2013, **21**, 12495–12506.
- 101 W. Zhang, M. Anaya, G. Lozano, M. E. Calvo, M. B. Johnston, H. Míguez and H. J. Snaith, *Nano Lett.*, 2015, **15**, 1698–1702.
- 102 B. Gholipour, G. Adamo, D. Cortecchia, H. N. S. Krishnamoorthy, M. D. Birowosuto, N. I. Zheludev and C. Soci, *Adv. Mater.*, 2017, **29**, 1604268.
- 103 T. Wood, M. Naffouti, J. Berthelot, T. David, J.-B. Claude, L. Métayer, A. Delobbe, L. Favre, A. Ronda, I. Berbezier, N. Bonod and M. Abbarchi, *ACS Photonics*, 2017, **4**, 873–883.
- 104 X. Zhu, W. Yan, U. Levy, N. A. Mortensen and A. Kristensen, *Sci. Adv.*, 2017, **3**, e1602487.
- 105 B. Yang, W. Liu, Z. Li, H. Cheng, D.-Y. Choi, S. Chen and J. Tian, *Nano Lett.*, 2019, DOI: 10.1021/acs.nanolett.8b04923.
- 106 V.-C. Su, C. H. Chu, G. Sun and D. P. Tsai, *Opt. Express*, 2018, **26**, 13148–13182.
- 107 H.-T. Chen, A. J. Taylor and N. Yu, *Rep. Prog. Phys.*, 2016, **79**, 076401.
- 108 J. Sautter, I. Staude, M. Decker, E. Rusak, D. N. Neshev, I. Brener and Y. S. Kivshar, *ACS Nano*, 2015, **9**, 4308–4315.
- 109 P. Gutruf, C. Zou, W. Withayachumnankul, M. Bhaskaran, S. Sriram and C. Fumeaux, *ACS Nano*, 2015, **10**, 133–141.
- 110 H. Cheng, S. Chen, P. Yu, W. Liu, Z. Li, J. Li, B. Xie and J. Tian, *Adv. Opt. Mater.*, 2015, **3**, 1744–1749.
- 111 M. Seo, J. Kyoung, H. Park, S. Koo, H.-S. Kim, H. Bernien, B. J. Kim, J. H. Choe, Y. H. Ahn, H.-T. Kim, N. Park, Q.-H. Park, K. Ahn and D.-S. Kim, *Nano Lett.*, 2010, **10**, 2064–2068.
- 112 J. Y. Ou, E. Plum, L. Jiang and N. I. Zheludev, *Nano Lett.*, 2011, **11**, 2142–2144.
- 113 A. Benz, I. Montano, J. F. Klem and I. Brener, *Appl. Phys. Lett.*, 2013, **103**, 263116.
- 114 I. M. Pryce, K. Aydin, Y. A. Kelaita, R. M. Briggs and H. A. Atwater, *Nano Lett.*, 2010, **10**, 4222–4227.

- 115 S.-I. Park, Y. Xiong, R.-H. Kim, P. Elvikis, M. Meitl, D.-H. Kim, J. Wu, J. Yoon, C.-J. Yu, Z. Liu, Y. Huang, K. Hwang, P. Ferreira, X. Li, K. Choquette and J. A. Rogers, *Science*, 2009, **325**, 977–981.
- 116 Y. Yao, R. Shankar, M. A. Kats, Y. Song, J. Kong, M. Loncar and F. Capasso, *Nano Lett.*, 2014, **14**, 6526–6532.
- 117 H.-S. Ee and R. Agarwal, *Nano Lett.*, 2016, **16**, 2818–2823.
- 118 M. L. Tseng, J. Yang, M. Semmlinger, C. Zhang, P. Nordlander and N. J. Halas, *Nano Lett.*, 2017, **17**, 6034–6039.
- 119 F. Sterl, N. Strohfeldt, R. Walter, R. Griessen, A. Tittl and H. Giessen, *Nano Lett.*, 2015, **15**, 7949–7955.
- 120 Y. Chen, X. Duan, M. Matuschek, Y. Zhou, F. Neubrech, H. Duan and N. Liu, *Nano Lett.*, 2017, **17**, 5555–5560.
- 121 X. Duan, S. Kamin and N. Liu, *Nat. Commun.*, 2017, **8**, 14606.
- 122 S. N. Burokur, J.-P. Daniel, P. Ratajczak and A. de Lustrac, *Appl. Phys. Lett.*, 2010, **97**, 064101.
- 123 Y. Lee, M.-K. Park, S. Kim, J. H. Shin, C. Moon, J. Y. Hwang, J.-C. Choi, H. Park, H.-R. Kim and J. E. Jang, *ACS Photonics*, 2017, **4**, 1954–1966.
- 124 M. Decker, C. Kremers, A. Minovich, I. Staude, A. E. Miroshnichenko, D. Chigrin, D. N. Neshev, C. Jagadish and Y. S. Kivshar, *Opt. Express*, 2013, **21**, 8879–8885.
- 125 O. Buchnev, N. Podoliak, M. Kaczmarek, N. I. Zheludev and V. A. Fedotov, *Adv. Opt. Mater.*, 2015, **3**, 674–679.
- 126 S. K. Deb and J. A. Chopoorian, *J. Appl. Phys.*, 1966, **37**, 4818–4825.
- 127 D. R. Rosseinsky and R. J. Mortimer, *Adv. Mater.*, 2011, **13**, 783–793.
- 128 A. A. Argun, P.-H. Aubert, B. C. Thompson, I. Schwendeman, C. L. Gaupp, J. Hwang, N. J. Pinto, D. B. Tanner, A. G. MacDiarmid and J. R. Reynolds, *Chem. Mater.*, 2004, **16**, 4401–4412.
- 129 T. Xu, E. C. Walter, A. Agrawal, C. Bohn, J. Velmurugan, W. Zhu, H. J. Lezec and A. A. Talin, *Nat. Commun.*, 2016, **7**, 10479.
- 130 S. D. Stranks and H. J. Snaith, *Nat. Nanotechnol.*, 2015, **10**, 391.
- 131 B. R. Sutherland and E. H. Sargent, *Nat. Photonics*, 2016, **10**, 295.
- 132 Y. Gao, C. Huang, C. Hao, S. Sun, L. Zhang, C. Zhang, Z. Duan, K. Wang, Z. Jin, N. Zhang, A. V. Kildishev, C.-W. Qiu, Q. Song and S. Xiao, *ACS Nano*, 2018, **12**, 8847–8854.
- 133 G. Wang, X. Chen, S. Liu, C. Wong and S. Chu, *ACS Nano*, 2016, **10**, 1788–1794.
- 134 J. Jang, H. Jeong, G. Hu, C.-W. Qiu, K. T. Nam and J. Rho, *Adv. Opt. Mater.*, 2018, 1801070.
- 135 S. Sun, W. Yang, C. Zhang, J. Jing, Y. Gao, X. Yu, Q. Song and S. Xiao, *ACS Nano*, 2018, **12**, 2151–2159.
- 136 J. Proust, F. Bedu, B. Gallas, I. Ozerov and N. Bonod, *ACS Nano*, 2016, **10**, 7761–7767.
- 137 R. Verre, N. Maccaferri, K. Fleischer, M. Svedendahl, N. O. Länk, A. Dmitriev, P. Vavassori, I. V. Shvets and M. Käll, *Nanoscale*, 2016, **8**, 10576–10581.
- 138 N. S. King, L. Liu, X. Yang, B. Cerjan, H. O. Everitt, P. Nordlander and N. J. Halas, *ACS Nano*, 2015, **9**, 10628–10636.
- 139 R. Fan, J. Zhu, W.-G. Wu and Y. Huang, *Small*, 2017, **13**, 1601710.